Temperature-dependent multiscale-dynamics in Lithium-Ion battery electrochemical models

Harikesh Arunachalam, *Student Member, IEEE,* Simona Onori, *Member, IEEE,* Ilenia Battiato

Abstract— In a Lithium-ion battery, the relative importance between the three microscale transport processes, i.e. diffusion, electromigration and heterogeneous reaction, can be quantified using the dimensionless Electric Péclet (Pe) and Damköhler (Da) numbers. By means of homogenization technique, we upscale the pore-scale Poisson-Nernst-Planck equation to the macroscopic scale and formulate a phase diagram in the (Da,Pe)-space that identifies the applicability conditions under which isothermal electrochemical macroscopic models provide an accurate description of the micro-scale dynamics [1]. In this work, we focus on the effect of temperature on macroscale (Newman-type) models' accuracy for a number of commercially available lithium-ion batteries. We show that macroscopic models are able to accurately represent pore-scale dynamics only within specific temperature bounds and their veracity is strongly controlled by the battery operating temperature conditions.

I. INTRODUCTION

Lithium-ion batteries have been extensively used as energy storage devices in portable electronics for their light weight and higher energy and power density properties in comparison with their metal-based counterparts [2]. Their applicability has been evolving towards large scale applications such as aircraft auxiliary power units, hybrid and fully electric vehicles, and long duration grid energy storage [3].

The transition from small scale electronics to electric vehicles with much higher power and energy demands has been hampered by the relative lack of understanding of scaling effects, which impact battery performance and electrochemical and mechanical responses [4]. Battery chemical and physical heterogeneity on a multiplicity of scales calls for the use of models that can capture the system multiscale dynamics, including physicochemical processes during battery charge/discharge operations, especially at high current rates [5]. Further, physics-based multiscale models must account for the effects of material properties and battery morphology [6].

A plethora of mathematical models have been developed to capture the transport phenomena inside a Lithium ion cell. They include empirical, thermal, stress-strain, molecular/atomistic, and electrochemical models [7]. Electrochemical models can be formulated at a variety of different scales, from the pore-scale (microscale) to the continuum scale (macroscale).

Microscale models consider diffusion, conduction, and electrochemical kinetics at the micrometer scale, and simulate ion transport in the electrodes and separator [8]. These models are computationally demanding [9] and have limited application in battery design since they focus primarily on localized phenomena without considering the cell-level behavior [10]. In comparison, macroscopic models are computationally efficient. For automotive applications, understanding macroscopic design features is essential

Harikesh Arunachalam is with the Automotive Engineering Department, Clemson University, Greenville, 29607, SC, USA. [harunac@g.clemson.edu]

Simona Onori is with the Automotive Engineering Department, Clemson University, Greenville, 29607, SC, USA. [sonori@clemson.edu]

Ilenia Battiato is with the Department of Mechanical Engineering, San Diego State University, San Diego, 92115, CA, USA. [ibattiato@mail.sdsu.edu]

in order to determine their impact on microscopic electrochemical processes [11]. This facilitates the need for a model combining these two scales, which interpret the behavior of the system and improve numerical efficiency.

The macroscopic lithium-ion battery model developed by Newman *et al.* [12] is the earliest developed and widely utilized electrochemical model today. This model was derived using the volume averaging technique, and treats the electrode as a homogeneous continuum. This model does not consider the microscopic structure of the electrode. Changes in the effective properties of the transport parameters such as ionic diffusion and conductivity are accounted for using a Bruggeman's relation [13].

Upscaling studies emphasize the derivation of effective models that incorporate the microscopic characteristics of the porous medium. To the best of our knowledge, upscaled models have not completely addressed the validity of the underlying assumptions and the approximations based on which they were derived. It is important for macroscopic models that have been developed with the objective of designing more accurate and predictive battery management systems (BMS) to address this aspect of modeling.

A multiple scale asymptotic expansion technique to upscale the microscopic mass and charge transport equations in a lithium ion battery model has been studied in [1]. Dimensionless Electric Péclet (Pe) and Damköhler (Da) numbers were defined to describe mass and charge transport of lithium ions in the electrolyte. Using a homogenization approach, constraints that identify a domain where the upscaled equations accurately describe the microscale processes were identified. A phase diagram in the (Pe,Da) space summarized mass transport in the electrolyte phase.

In the process of developing a more predictive model, there is a need to identify operating conditions where effective macroscale transport equations would break down. This aspect of modeling will be addressed in this paper. The focus of this paper is to apply the results obtained in [1] to understand the veracity of mathematical models that describe lithium-ion battery dynamics. In order to do that, we have computed the values of Pe and Da for different battery electrode chemistries reported in literature. The parameters α and β are obtained from these dimensionless parameters, as a function of the scale separating parameter ε.

This information is studied using the phase diagram for different battery operating temperatures. The location of the data points (α, β) determines the applicability of the upscaled transport equations in the electrolyte medium. The key advantage of the work presented in this paper is that we can determine a priori whether an electrochemical macroscopic model would be capable of describing the microscale dynamics of a particular battery system at a given operating condition.

In Section II, a summary of the homogenization technique that was implemented in the derivation of our isothermal macroscopic model to describe lithium ion transport in the battery medium is presented [1]. In Section IV, we present the dimensionless parameters computed for different battery chemistries reported in literature, and investigate the effect of operating temperature on the applicability of the macroscale transport equations. In the process,

we interpret the behavior of the system by examining the variation in the battery parameters with the operating conditions. Section V summarizes the conclusion of this work.

II. PORE-SCALE EQUATIONS

Batteries are composed of a solid porous medium (the electrode phase) and a fluid (the electrolyte phase) separated by an interface. The electrolyte solution surrounds the electrode and fills the void spaces of the porous matrix. The electrolyte is a binary lithium salt dissolved in an organic solvent. Diffusion and electro-migration are the primary transport mechanisms lithium-ion transport in the electrolyte phase. Reaction occurs at the electrode-electrolyte interface Γ^ε. The electrochemical model is developed for an isothermal case, and does not include the energy balance equation.

Let us assume active particles inside an electrode are microscopically arranged in the medium in the form of spatially periodic unit cells Y with a characteristic length $\varepsilon \equiv \ell/L \ll 1$, where ℓ represents the microscopic length scale and L represents the macroscopic length scale. The parameter ε is called the scale-separation variable, and is the ratio of characteristic lengths associated with the micro and macro scales. The unit cell consists of the electrolyte space $\mathcal{B}$ and the ion permeable solid matrix $\mathcal{S}$ that are separated by the smooth surface Γ. Fig. 1 presents an illustration of the unit cell and the porous medium of the lithium ion battery. $\mathbf{x}$ and $\mathbf{y}$ represent the coordinate system variables at the macroscale and microscale, respectively, while t represents the time variable.

The mass and charge transport equations in the electrolyte and the electrode phases control the spatiotemporal evolution of the concentration of Lithium ions $\hat{c}^i_\varepsilon(\mathbf{x}, t)$ $[\text{mol}L^{-3}]$ and the electrostatic potential $\hat{\phi}^i_\varepsilon(\mathbf{x}, t)$ $[V]$ in the active particles $\{i = s\}$ and the electrolyte $\{i = e\}$.
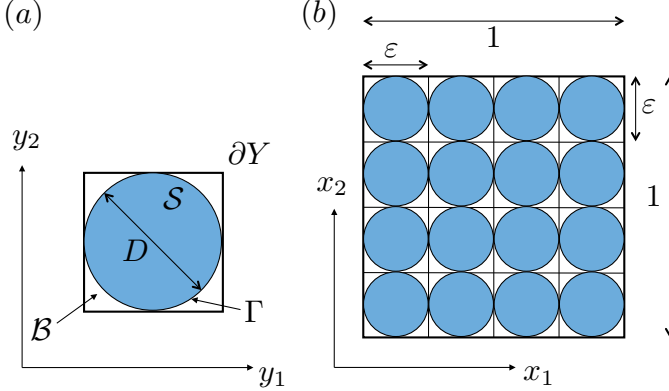
Fig. 1: Representation of an single unit cell (a), and a porous medium idealized as a periodic arrangement of repeating unit cells (b).

A. Transport Processes and Dimensionless Numbers

The transport processes occurring at the pore-scale include heterogenous reaction on the electrode-electrolyte interface Γ^ε, and ion diffusion and migration in the electrode and electrolyte phases, $\mathcal{S}^\varepsilon$ and $\mathcal{B}^\varepsilon$, respectively. The characteristic time scales associated with the heterogeneous reaction, ionic diffusion, and ionic migration over a macroscopic length scale L are

$$\hat{t}_R = \frac{LF}{k}, \quad \hat{t}_{D_i} = \frac{L^2}{D^i}, \quad \hat{t}_{M_i} = \frac{L^2 F^2 c^s_{\max}}{RTK^i}, \quad i = \{e, s\}, \quad (1)$$

respectively. In (1), T is the absolute temperature; F is Faraday's constant and R is the universal gas constant; k $[LV\Omega^{-1}\text{mol}^{-1}]$ is the electrochemical reaction rate constant of Lithium ion transfer on Γ^ε; $D^i = \mathcal{O}(\hat{D}^i)$ $[L^2 T^{-1}]$ and $K^i = \mathcal{O}(\hat{K}^i)$ $[\Omega^{-1}L^{-1}]$, $i =$

$\{e, s\}$, are characteristic values of the inter-diffusion and electric conductivity tensors $\hat{D}^i$ and $\hat{K}^i$ in the electrode ($i = s$) and the electrolyte ($i = s$), respectively ($\mathcal{O}$ represents the order of the variable under discussion); $c^s_{\max}$ is the maximum concentration of Lithium that can be stored in the active particle;

We define the dimensionless Damköhler and electric Péclet numbers as

$$\text{Da}_i := \frac{\hat{t}_{D_i}}{\hat{t}_R} = \frac{Lk}{FD^i} \quad \text{and} \quad \text{Pe}_i := \frac{\hat{t}_{D_i}}{\hat{t}_{M_i}} = \frac{RTK^i}{D^i F^2 c^s_{\max}}, \quad (2)$$

$i = \{e, s\}$. They provide information about the relative magnitude of ion transport processes in the electrolyte and the electrode phases.

B. Electrolyte Phase

The dimensionless mass and charge transport equations in the electrolyte phase $\mathbf{x} \in \mathcal{B}^\varepsilon$ are

$$\frac{\partial c^e_\varepsilon}{\partial t_e} = \nabla \cdot [(\mathbf{D}^e + \lambda t^2_+ \text{Pe}_e \mathbf{K}^e / c^e_\varepsilon) \nabla c^e_\varepsilon + 2\text{Pe}_e t_+ \mathbf{K}^e \nabla \phi^e_\varepsilon], \quad (3a)$$

$$0 = \nabla \cdot [(\lambda t_+ \text{Pe}_e \mathbf{K}^e / c^e_\varepsilon) \nabla c^e_\varepsilon + 2\text{Pe}_e \mathbf{K}^e \nabla \phi^e_\varepsilon], \quad (3b)$$

subject to

$$\mathbf{n}_e \cdot [(\mathbf{D}^e + \lambda t^2_+ \text{Pe}_e \mathbf{K}^e / c^e_\varepsilon) \nabla c^e_\varepsilon + 2\text{Pe}_e \, t_+ \mathbf{K}^e \nabla \phi^e_\varepsilon]$$
$$= \text{Da}_e f(c^e_\varepsilon, c^s_\varepsilon, \phi^s_\varepsilon, \phi^e_\varepsilon), \quad \mathbf{x} \in \Gamma^\varepsilon, \quad (4a)$$

$$\mathbf{n}_e \cdot [(\text{Pe}_e \lambda t_+ \mathbf{K}^e / c^e_\varepsilon) \nabla c^e_\varepsilon + 2\text{Pe}_e \mathbf{K}^e \nabla \phi^e_\varepsilon]$$
$$= \text{Da}_e f(c^e_\varepsilon, c^s_\varepsilon, \phi^s_\varepsilon, \phi^e_\varepsilon), \quad \mathbf{x} \in \Gamma^\varepsilon, \quad (4b)$$

respectively. In (3) and (4), $\mathbf{D}^e = \hat{\mathbf{D}}^e / D^e$ and $\mathbf{K}^e = \hat{\mathbf{K}}^e / K^e$ are the dimensionless inter-diffusion coefficient and the electric conductivity in the electrolyte, respectively; $f(c^e_\varepsilon, c^s_\varepsilon, \phi^s_\varepsilon, \phi^e_\varepsilon) = \sqrt{c^e_\varepsilon c^s_\varepsilon (1 - c^s_\varepsilon)} \{\exp(\phi^s_\varepsilon - \phi^e_\varepsilon - U) - \exp[-(\phi^s_\varepsilon - \phi^e_\varepsilon - U)]\}$; $U = F\hat{U}/(2RT)$ and $\hat{U}$ are the dimensionless and dimensional open circuit potentials, respectively; t_+ is the transference number, $\lambda = 1 + \partial_{\ln \hat{c}^e_\varepsilon} \ln f_\pm$ is assumed constant and $f_\pm$ is the activity coefficient. $\mathbf{n}_e$ is the outward unit normal vector to Γ^ε pointing from the electrolyte towards the active particle. The dimensional spatial and time scales ($\hat{\mathbf{x}}$ and $\hat{t}$) are non-dimensionalized by the macroscopic length L and the diffusion time in the electrolyte phase $\hat{t}_{D_e}$ respectively, i.e. $\mathbf{x} = \hat{\mathbf{x}}/L$ and $t_e = \hat{t}/\hat{t}_{D_e}$.

C. Electrode Phase

The dimensionless mass and charge transport equations in the electrode phase $\mathcal{S}^\varepsilon$ can be written as

$$\frac{\partial c^s_\varepsilon}{\partial t_s} = \nabla \cdot (\mathbf{D}^s \nabla c^s_\varepsilon), \qquad \mathbf{x} \in \mathcal{S}^\varepsilon, \quad (5a)$$

$$0 = \nabla \cdot (\text{Pe}_s \mathbf{K}^s \nabla \phi^s_\varepsilon), \qquad \mathbf{x} \in \mathcal{S}^\varepsilon, \quad (5b)$$

subject to

$$-\mathbf{n}_s \cdot [\mathbf{D}^s \nabla c^s_\varepsilon] = \text{Da}_s f(c^e_\varepsilon, c^s_\varepsilon, \phi^s_\varepsilon, \phi^e_\varepsilon) \qquad \mathbf{x} \in \Gamma^\varepsilon, \quad (6a)$$

$$-\mathbf{n}_s \cdot [2\text{Pe}_s \mathbf{K}^s \nabla \phi^s_\varepsilon] = \text{Da}_s f(c^e_\varepsilon, c^s_\varepsilon, \phi^s_\varepsilon, \phi^e_\varepsilon) \qquad \mathbf{x} \in \Gamma^\varepsilon, \quad (6b)$$

respectively. In (5) and (6), $c^i_\varepsilon := \hat{c}^i_\varepsilon / c^s_{\max}$ and $\phi^i_\varepsilon := \hat{\phi}^i_\varepsilon F/(2RT)$ $i = \{s, e\}$, are the dimensionless concentration of Lithium ions and the electrostatic potential in the active particles $\{i = s\}$ and the electrolyte $\{i = e\}$; $\mathbf{n}_s$ is the outward unit normal vector to Γ^ε pointing from the active particle towards the electrolyte. The dimensional spatial and time scales ($\hat{\mathbf{x}}$ and $\hat{t}$) are non-dimensionalized by the macroscopic length L and the diffusion time in the solid phase $\hat{t}_{D_s}$ respectively, i.e. $\mathbf{x} = \hat{\mathbf{x}}/L$ and $t_s = \hat{t}/\hat{t}_{D_s}$.

III. CONTINUUM-SCALE EQUATIONS

Continuum-scale equations govern the spatiotemporal distribution of averaged concentration of Lithium ions and the electrostatic

potential in the active particles and the electrolyte. We define the following local averages of a quantity $\mathcal{A}(\mathbf{x})$ in the electrode and electrolyte phases:

$$\langle \mathcal{A}\rangle_e \equiv \frac{1}{|Y|}\int_{\mathcal{B}(\mathbf{x})}\mathcal{A}\mathrm{d}\mathbf{y}, \quad \langle \mathcal{A}\rangle_s \equiv \frac{1}{|Y|}\int_{\mathcal{S}(\mathbf{x})}\mathcal{A}\mathrm{d}\mathbf{y}, \quad \langle \mathcal{A}\rangle_\mathcal{B} \equiv \frac{1}{|\mathcal{B}|}\int_{\mathcal{B}(\mathbf{x})}\mathcal{A}\mathrm{d}\mathbf{y} \tag{7}$$

where $\langle \mathcal{A}\rangle = \eta\langle \mathcal{A}\rangle_\mathcal{B}$ and $\eta = |\mathcal{B}|/|Y|$ is the porosity. A system of equations governing the dynamics of (7) can be obtained by means of upscaling techniques. Using the method of multiple-scale expansions, we expand the concentration and potential c_ε^i and ϕ_ε^i, $i = \{e, s\}$ in equations (3)-(6) into an asymptotic series in powers of ε. We define exponents α, β, γ and δ as

$$\mathrm{Pe}_e = \varepsilon^{-\alpha}, \quad \mathrm{Da}_e = \varepsilon^\beta, \quad \mathrm{Da}_s = \varepsilon^\gamma, \quad \mathrm{Pe}_s = \varepsilon^{-\delta}. \tag{8}$$

in order to understand the system behaviour.

In [1], we show that pore-scale reactive transport processes described by (3a)–(4b) can be homogenized, i.e., approximated up to order ε^2 in the electrolyte phase with the following effective mass and charge transport equations:

$$\eta\frac{\partial\langle c_\varepsilon^e\rangle_\mathcal{B}}{\partial t_e} = \nabla_\mathbf{x}\cdot\mathbf{D}^e\nabla_\mathbf{x}\langle c_\varepsilon^e\rangle_\mathcal{B} + \mathrm{Pe}_e\nabla_\mathbf{x}\cdot(\mathbf{K}_1^e\nabla_\mathbf{x}\ln\langle c_\varepsilon^e\rangle_\mathcal{B}$$
$$+ 2\mathbf{K}_2^e\nabla_\mathbf{x}\langle\phi_\varepsilon^e\rangle_\mathcal{B}) + \varepsilon^{-1}\mathrm{Da}_e\eta\,\mathscr{K}^\star f(\langle c_\varepsilon^e\rangle_\mathcal{B}, \langle c_\varepsilon^s\rangle_s, \langle\phi_\varepsilon^e\rangle_\mathcal{B}, \langle\phi_\varepsilon^s\rangle_s) \tag{9}$$

and

$$\mathrm{Pe}_e\nabla_\mathbf{x}\cdot(\mathbf{K}_1^{e\star}\nabla_\mathbf{x}\ln\langle c_\varepsilon^e\rangle_\mathcal{B} + 2\mathbf{K}_2^{e\star}\nabla_\mathbf{x}\langle\phi_\varepsilon^e\rangle_\mathcal{B})$$
$$= -\varepsilon^{-1}\mathrm{Da}_e\,\eta\,\mathscr{K}^\star f(\langle c_\varepsilon^e\rangle_\mathcal{B}, \langle c_\varepsilon^s\rangle_s, \langle\phi_\varepsilon^e\rangle_\mathcal{B}, \langle\phi_\varepsilon^s\rangle_s) \tag{10}$$

provided the following conditions are met,

1) $\mathrm{Da}_e < 1$,
2) $\mathrm{Pe}_e < 1$,
3) $\mathrm{Da}_e/\mathrm{Pe}_e < 1$,

and $\varepsilon \ll 1$. In (9)-(10), $\mathbf{D}^e$, $\mathbf{K}_1^e$, $\mathbf{K}_2^e$, $\mathbf{K}_1^{e,\star}$, $\mathbf{K}_2^{e,\star}$, and $\mathscr{K}^\star$ are effective coefficients. Similarly, for the electrode phase,

$$\frac{\partial\langle c_\varepsilon^s\rangle_s}{\partial t_s} = \nabla_\mathbf{x}\cdot\left(\mathbf{D}^s\nabla_\mathbf{x}\langle c_\varepsilon^s\rangle_s\right)$$
$$- \varepsilon^{-1}\mathrm{Da}_2\,\eta\,\mathscr{K}^\star f(\langle c_\varepsilon^e\rangle_\mathcal{B}, \langle c_\varepsilon^s\rangle_s, \langle\phi_\varepsilon^e\rangle_\mathcal{B}, \langle\phi_\varepsilon^s\rangle_s) \tag{11}$$

and

$$2\mathrm{Pe}_2\,\nabla_\mathbf{x}\cdot(\mathbf{K}^s\nabla_\mathbf{x}\langle\phi_\varepsilon^s\rangle_s) =$$
$$\varepsilon^{-1}\mathrm{Da}_s\,\eta\,\mathscr{K}^\star f(\langle c_\varepsilon^e\rangle_\mathcal{B}, \langle c_\varepsilon^s\rangle_s, \langle\phi_\varepsilon^e\rangle_\mathcal{B}, \langle\phi_\varepsilon^s\rangle_s) \tag{12}$$

provided the following conditions are met

1) $\mathrm{Da}_s < 1$,
2) $\mathrm{Da}_s/\mathrm{Pe}_s < 1$.

In (11)-(12) $\mathbf{D}^s$ and $\mathbf{K}^s$ are effective parameters.

The former conditions enforce bounds on the order of magnitude of relevant dimensionless numbers that describe transport processes dynamics. The former conditions can be expressed in more compact form in terms of bounds on the magnitude of α and β, which can be summarized in the form of a phase diagram of the type showed in Fig. 2. In the region shaded grey, the established conditions are valid and the macroscopic equation holds. In the white region, micro and macro scale equations are coupled and must be solved simultaneously. At the point $(\alpha, \beta) = (0, 0)$, the transport mechanisms are of the same order of magnitude. This approach enables us to define a domain where upscaled Newman-type macroscopic equations are capable of accurately describing the microscale processes. When they fail to capture the system

response, processes at the microscale and macroscale cannot be decoupled. In the latter case, multi-algorithm, hybrid techniques should be employed instead.

Finally we notice that, despite classical macroscopic models as the one just described are derived for isothermal conditions, our analysis suggests that coupling across scales may occur if the battery is operated at different temperatures. Because of (2), constraints on Pe_e result in bounds on the maximum temperature when multiscale, coupled effects will impact the accuracy of standard Newman's type models.

In the following, we consider a number of commercial batteries with different chemical composition and investigate in what portion of the parameter space they follow. This information is critical to establish the appropriateness of modeling approaches to be employed when simulating a system with electrochemical models. Further, we investigate the impact of temperature on determining the degree of coupling between pore-scale and macroscale transport processes.

Without loss of generality, we focus on the impact of temperature on process coupling in the electrolyte only.
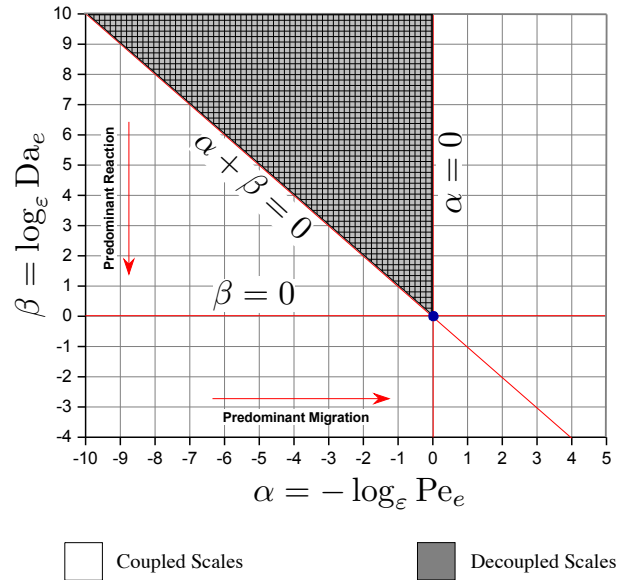
Fig. 2: *Phase diagram that specifies the range of applicability of the upscaled equation in the electrolyte phase.*

IV. ANALYSIS OF BATTERY CHEMICAL COMPOSITION AND TEMPERATURE DEPENDENT DYNAMICS

In this section, we examine the operating parameters of existing batteries reported in literature and determine the corresponding values of the dimensionless parameters α and β. This information will allow one to determine whether or not Newman-type macroscopic models are the most appropriate modeling tools.

The key parameters of interest in this study are:

1) electrochemical reaction rate constant, k [A $\cdot$ m$^{2.5}\cdot$mol$^{-1.5}$];
2) lithium diffusion coefficient in the electrolyte D^e [m$^2\cdot$s^{-1}];
3) lithium ionic conductivity of in the electrolyte K^e [S $\cdot$m^{-1}];
4) and battery operating temperature, T [K].
5) dimensionless scale separation parameter, $\varepsilon = \ell/L$
6) maximum concentration of lithium in an electrode, $c_{\max}^s$ [mol $\cdot$ m^{-3}].
7) F, Faraday constant, whose value is $96,485$ $A \cdot s \cdot$ mol^{-1}.

8) R, the universal gas constant, whose value is 8.314 $J \cdot mol^{-1} \cdot K^{-1}$.

In the electrolyte phase, we treat the separator as an inherent property of the electrolyte. For this reason, the value for the macroscale characteristic length L is taken as the combined thickness of the electrode and separator, expressed in m. The value for the microscale characteristic length ℓ is taken as the average diameter of the active particle in the electrode, expressed in m. This is illustrated in the representation of the unit cell in figure 1.

The values of ℓ, L, c^s_{max}, R, and F are considered invariant with respect to temperature for the sake of this study. We proceed to investigate the effect of temperature on the parameters k, K^e, and D^e.

Our initial study involves plotting the data points (α,β) in the phase diagram for eight different battery electrode chemistries whose key parameters have been provided under room temperature conditions (25°C or 298K). This is shown in figure 3. These battery compositions have been chosen because they consist of the most commonly used cathode materials in commercial lithium-ion batteries. The first battery system consists of a lithium graphite
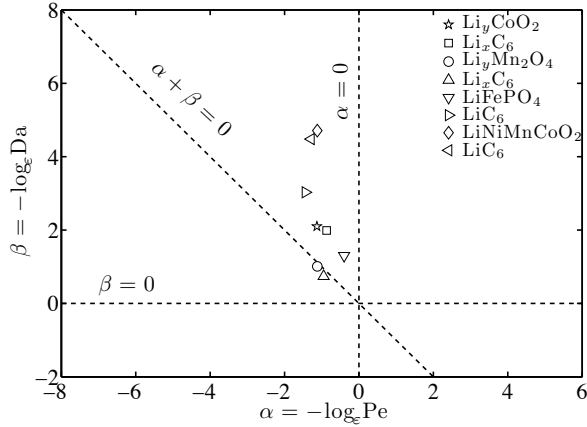
Fig. 3: Representation in the phase diagram of dimensionless parameters α and β for the most commonly used lithium-ion battery materials. These values are determined at room temperature.

negative electrode (Li_xC_6) and a lithium cobalt oxide (LCO) positive electrode (Li_yCoO_2), and the electrolyte is composed of 1.2 M of $LiPF_6$ salt dissolved in a 1:2 v/v mixture of ethylene carbonate and dimethyl carbonate (EC:2DMC). All parameter values for this system have been obtained from [14] and [15]. The second battery system consists of a lithium carbon negative electrode (Li_xC_6) and a lithium manganese oxide (LMO) positive electrode ($Li_yMn_2O_4$), and the polymer electrolyte is comprised of $LiClO_4$ salt dissolved in poly(ethylene oxide) (PEO). Parameter values for this system have been obtained from [16] and [17].

The third battery system consists of a lithium graphite negative electrode (LiC_6) and a lithium ferrous phosphate (LFP) positive electrode ($LiFePO_4$). The parameter values have been procured from [18]. The fourth battery chemistry is composed of lithium carbon negative electrode (LiC_6) and a lithium nickel manganese cobalt oxide (Li NMC) positive electrode ($LiNi_{1/3}Mn_{1/3}Co_{1/3}O_2$). The parameter values have been acquired from [19].

We observe in the phase diagram of figure 3 that the battery systems composed of $LiFePO_4$, Li_yCoO_2, and $LiNi_{1/3}Mn_{1/3}Co_{1/3}O_2$ have parameters that fall in the shaded region of our phase diagram in figure 1. This implies that the macroscale mass transport equation

is capable of describing the porous medium composed of these materials. However, the system containing $Li_yMn_2O_4$ cathode and Li_xC_6 anode must also utilize the microscale equations in order to describe the electrochemical dynamics in the medium. When compared with the other three chemistries, this observation is attributed to a combination of two factors: the lower value of the scaling parameter ε coupled with faster kinetics of lithium transport at the reaction interface. This implies that the active material and porous electrode structure play an important role in determining the validity of the electrochemical model at a given operating condition.

To emphasize the importance of these two factors, we present another lithium ion battery chemistry composed of lithium manganate cathode and lithium graphite anode. The electrolyte is composed of 1.0 M of $LiPF_6$ salt dissolved in a 3:7 v/v mixture of ethylene carbonate and ethyl methyl carbonate (3EC:7EMC). The values for ionic conductivity in the electrolyte have been reported as a function of temperature in [20]. Valøen and Reimers have reported the variation in the ionic diffusion coefficient for this system for different temperatures in [21]. By applying a cubic spline interpolation, we compute the values of ionic diffusivity for intermediate operating temperatures in the region of our interest. The values we have obtained are in agreement with those reported by Nyman *et al.* in [22].

The electrochemical reaction rate constant k for a given electrode system can be described as a function of temperature using the Arrhenius equation, as reported in [23] and [24]:

$$k_j(T) = k_{j,ref} \cdot exp\left[\frac{Ea_{r,j}}{R}\left(\frac{1}{T_{ref}} - \frac{1}{T}\right)\right]. \quad (13)$$

$k_j(T)$ and $k_{j,ref}$ are the reaction rate constants of electrode j at the desired temperature T and reference temperature T_{ref}, respectively. $Ea_{r,j}$ is the reaction rate activation energy of electrode j. For our system of interest, the values of $k_{j,ref}$ and $Ea_{r,j}$ are provided in [25] for a reference temperature of 298K (25°C). The parameter values necessary to determine α and β for this system are also presented here. Using (13), we compute the values of k for different temperatures of our interest.

The phase diagrams for lithium graphite and lithium manganate are presented in figures 4 and 5, respectively. In this case, both the systems exhibit a similar behavior. The magnitude of parameters α and β increase at a nearly equal rate with the operating temperature, since a line joining these data points would almost be parallel with the line $\alpha + \beta = 0$. This indicates that the behavior of the system (as a function of temperature) is a linear function in α and β. At elevated temperatures, the effect of increase in k is compensated by the increase in D^e, leading to only a small change in β. Similarly, the small change in α at elevated temperatures is a result of increase in K^e compensated by increase in D^e. For these systems, the data points satisfy the constraints on α and β over the range of operating temperature conditions. Hence our upscaled equation for lithium mass transport should provide an accurate description of the porescale behavior.

For the system described above, increasing temperature caused the data points (α,β) to propagate further within the domain of interest for the upscaled equation. It is also possible for the dimensionless parameters to exhibit a contrasting behavior. We present such a case by investigating the effect of increasing temperature for three different cathode chemistries: Li NMC, LFP, and LCO. The electrolyte used in these systems consists of $LiPF_6$ salt dissolved in an organic solvent mixture of propylene carbonate (PC), EC, and DMC.

The parameters necessary to compute α and β for the Li NMC battery system are derived from [26]. The electrolyte material
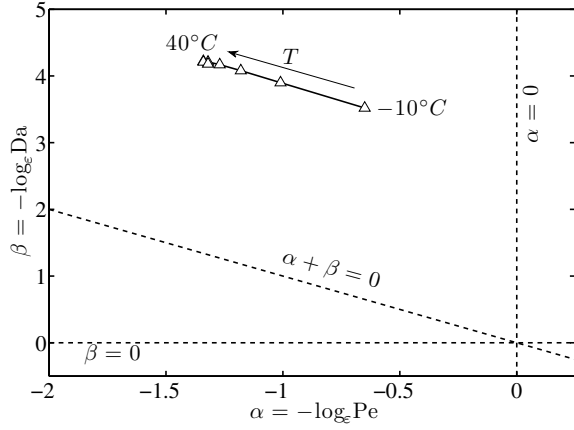
Fig. 4: Representation of parameters α and β in the phase diagram for Li_xC_6 anode as a function of temperature.
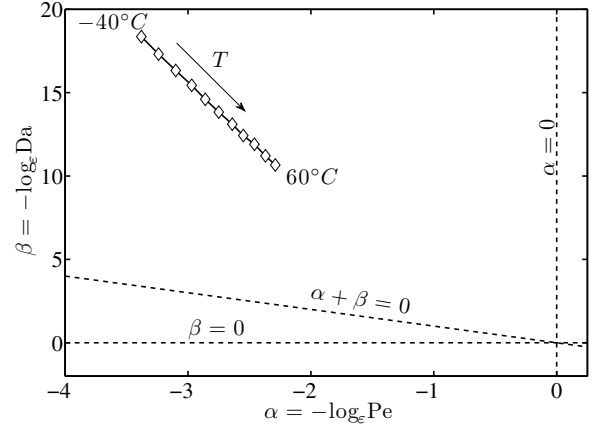
Fig. 6: Representation of parameters α and β in the phase diagram for $LiNiMnCoO_2$ cathode as a function of temperature.
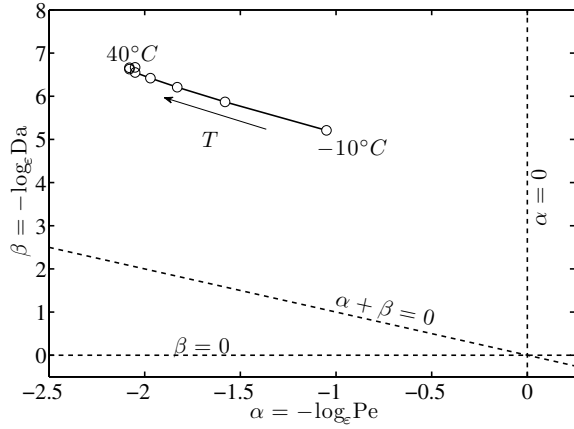
Fig. 5: Representation of parameters α and β in the phase diagram for $LiMn_2O_4$ cathode as a function of temperature.
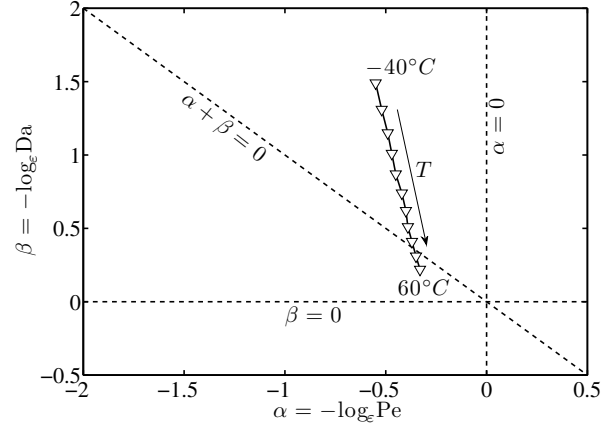
Fig. 7: Representation of parameters α and β in the phase diagram for $LiFePO_4$ cathode as a function of temperature.

is common for all the three cathode materials, hence the ionic diffusivity D^e and ionic conductivity K^e equations for LFP and LCO have also been utilized from [26].

The phase diagram for the lithium nickel manganese cobalt oxide cathode system is presented in figure 6. Values for the reaction rate constant k for LFP are determined using the Arrhenius equation (13). The parameter values for LFP are provided in [18] and the value of the reaction rate activation energy is obtained from [27]. The phase diagram for the lithium ferrous phosphate cathode system is presented in figure 7. The reaction rate constant expression (13) is also used for the LCO sustem. The parameter values for LCO are provided in [28] and the value of the reaction rate activation energy is obtained from [29]. The phase diagram for the lithium cobalt oxide cathode system is presented in figure 8.

In analyzing the phase diagrams in figures 6 to 8, we observe that for all the three cathode systems, the value of α increased and the value of β decreased with increasing operating temperature. In comparing the values of k for the Li NMC, LFP, and LCO, the relatively very slow kinetics of reaction at the Li NMC - electrolyte interface resulted in significantly higher values for β for this system. For the LFP and LCO systems, the kinetics of the interface reaction were several order of magnitude higher than the Li NMC system,
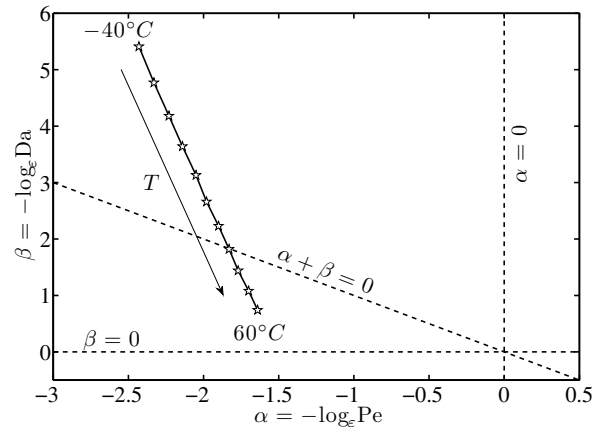
Fig. 8: Representation of parameters α and β in the phase diagram for $LiCoO_2$ cathode as a function of temperature.

and with increasing temperature, the rate of decrease in β was higher than the rate of increase in α.

We note that the upscaled equation of mass transport for the Li

NMC system is valid for the entire range of operating temperatures considered. However, for the LFP system, the macroscale equation is no longer accurate in describing microscale transport processes at temperatures 323K ($50°C$) and higher. For the LCO system, beyond 303K ($30°C$), the microscale equation of mass transport must be simultaneously solved with the upscaled equation. This is because the value of $\alpha + \beta$ is less than 0.

For the battery chemical compositions considered in this study, we observed that α and β vary linearly with temperature. The key transport parameters k, K^e, and D^e exhibit an exponential behavior with temperature, and the logarithmic dependence of α and β on the scale separating parameter ε results in a linear relationship of the data points with temperature. The Li-NMC system can be represented in the transport regime where diffusion and migration are of the same order (comparable) and dominate the reaction transport mechanism. The upscaled equations of such systems can also be reduced to a simpler form. The LFP and LCO system are represented in the transport regime where all three lithium transport processes are of the same order. Macroscale equations describing such systems are vulnerable to the effect of the operating temperature and may fail to describe battery physics at the microscopic level.

We would like to explicitly state that the parameter values k, K^e, and D^e required to determine Pe and Da are based on data values reported in literature, without any extrapolation. Figures 6 to 8 were investigated in the temperature range [233 - 333K], i.e., [-10 - 40°C] due to availability of data in this temperature range. Further experiments over a wider range of temperatures may enable the determination of these parameters, leading to the investigation of figures 4 and 5 beyond its currently reported temperature range.

V. Conclusions

Phase diagram in the (Pe$_e$, Da$_e$) space is used to examine the temperature-dependent dynamics in lithium-ion battery electrodes. Different battery compositions are examined to determine the range of applicability of classical Newman-type (macroscopic) models. The significant outcome of this work is the identification of temperature as a critical parameter that governs transport processes and induces the onset of multiscale dynamics. We also demonstrate that standard macroscopic models may fail to describe microscale processes in batteries that are operated above critical temperature conditions. Appropriate incorporation of this dependence will help in deriving more predictive battery models for different battery compositions.

References

[1] H. Arunachalam, S. Onori, and I. Battiato, "On Veracity of Macroscopic Lithium-Ion Battery Models," *J. Electrochem. Soc.*, vol. (submitted), no. JES-15-0382, 2015.

[2] W. Waag, C. Fleischer, and D. U. Sauer, "Critical review of the methods for monitoring of lithium-ion batteries in electric and hybrid vehicles," *Journal of Power Sources*, 2014.

[3] G. Pistoia, *Lithium Ion Batteries Advances and Applications*. Elsevier, Oxford, 2014.

[4] K.-J. Lee, K. Smith, A. Pesaran, and G.-H. Kim, "Three dimensional thermal-, electrical-, and electrochemical-coupled model for cylindrical wound large format lithium-ion batteries," *Journal of Power Sources*, 2013.

[5] M. Guo, G.-H. Kim, and R. E. White, "A three-dimensional multi-physics model for a Li-ion battery," *Journal of Power Sources*, 2013.

[6] W. Du, A. Gupta, X. Zhang, A. M. Sastry, and W. Shyy, "Effect of cycling rate, particle size and transport properties on lithium-ion cathode performance," *International Journal of Heat and Mass Transfer*, 2010.

[7] V. Ramadesigan, P. W. C. Northrop, S. De, S. Santhanagopalan, R. D. Braatz, and V. R. Subramanian, "Modeling and Simulation of Lithium-Ion Batteries from a Systems Engineering Perspective," *Journal of the Electrochemical Society*, 2012.

[8] G. B. Less, J. H. Seo, S. Han, A. M. Sastry, J. Zausch, A. Latz, S. Schmidt, C. Weiser, D. Kehrwald, and S. Fell, "Micro-Scale Modeling of Li-Ion Batteries: Parameterization and Validation," *Journal of the Electrochemical Society*, 2012.

[9] X. Zhang, "Multiscale Modeling of Li-Ion Cells: Mechanics, Heat Generation and Electrochemical Kinetics," Ph.D. dissertation, The University of Michigan, 2009.

[10] W. Du, N. Xue, W. Shyy, and J. R. R. A. Martins, "A Surrogate-Based Multi-Scale Model for Mass Transport and Electrochemical Kinetics in Lithium-Ion Battery Electrodes," *Journal of the Electrochemical Society*, 2014.

[11] G.-H. Kim, K. Smith, K.-J. Lee, S. Santhanagopalan, and A. Pesaran, "Multi-Domain Modeling of Lithium-Ion Batteries Encompassing Multi-Physics in Varied Length Scales," *Journal of the Electrochemical Society*, 2011.

[12] M. Doyle and J. Newman, "The use of Mathematical Modeling in the design of Lithium/Polymer Battery Systems," *Electrochimica Acta*, 1995.

[13] N. Xue, W. Du, A. Gupta, W. Shyy, A. M. Sastry, and J. R. R. A. Martins, "Optimization of a Single Lithium-Ion Battery Cell with a Gradient-Based Algorithm," *Journal of the Electrochemical Society*, 2013.

[14] M. Tang, P. Albertus, and J. Newman, "Two-Dimensional Modeling of Lithium Deposition during Cell Charging," *Journal of the Electrochemical Society*, 2009.

[15] G. F. Kennell and R. W. Evitts, "Two-Dimensional Lithium-Ion Battery Modeling with Electrolyte and Cathode Extensions," *Advances in Chemical Engineering and Science*, 2012.

[16] C.-W. Wang and A. M. Sastry, "Mesoscale Modeling of a Li-Ion Polymer Cell," *Journal of the Electrochemical Society*, 2007.

[17] S. Mazumder and J. Lu, "Faster-Than-Real-Time Simulation of Lithium Ion Batteries with Full Spatial and Temporal Resolution," *International Journal of Electrochemistry*, 2013.

[18] P. Gambhire, K. S. Hariharan, A. Khandelwal, S. M. Kolake, T. Yeo, and S. Doo, "A physics based reduced order aging model for lithium-ion cells with phase change," *Journal of Power Sources*, 2014.

[19] J. Marcicki, "Modeling, Parametrization, and Diagnostics for Lithium-Ion Batteries with Automotive Applications," Ph.D. dissertation, The Ohio State University, 2012.

[20] T. R. Jou, K. Xu, O. Borodin, and M. Ue, *Electrolytes for Lithium and Lithium-Ion Batteries*. Springer, Newyork, 2014.

[21] L. O. Valøen and J. N. Reimers, "Transport Properties of LiPF$_6$-Based Li-Ion Battery Electrolytes," *Journal of the Electrochemical Society*, 2005.

[22] A. Nyman, M. Behm, and G. Lindbergh, "Electrochemical characterisation and modelling of the mass transport phenomena in LiPF$_6$–EC–EMC electrolyte," *Electrochimica Acta*, 2008.

[23] M. Guo, G. Sikha, and R. E. White, "Single-Particle Model for a Lithium-Ion Cell: Thermal Behavior," *Journal of the Electrochemical Society*, 2011.

[24] E. Prada, D. D. Domenico, Y. Creff, J. Bernard, V. Sauvant-Moynot, and F. Huet, "Simplified Electrochemical and Thermal Model of LiFePO$_4$-Graphite Li-Ion Batteries for Fast Charge Applications," *Journal of the Electrochemical Society*, 2012.

[25] U. Kumar, A. K. Metya, N. Ramakrishnan, and J. K. Singh, "A Study of Transport Properties and Stress Analysis Using Atomistic and Macro Simulations for Lithium-Ion Batteries," *Journal of the Electrochemical Society*, 2014.

[26] S. Tippmann, D. Walper, L. Balboa, B. Spier, and W. G. Bessler, "Low-temperature charging of lithium-ion cells part I: Electrochemical modeling and experimental investigation of degradation behavior," *Journal of Power Sources*, 2014.

[27] M. Takahashi, S. Tobishima, K. Takei, and Y. Sakurai, "Reaction behavior of LiFePO$_4$ as a cathode material for rechargeable lithium batteries," *Solid State Ionics*, 2002.

[28] G. Sikha, R. E. White, and B. N. Popov, "A Mathematical Model for a Lithium-Ion Battery/Electrochemical Capacitor Hybrid System," *Journal of the Electrochemical Society*, 2005.

[29] X.-Y. Qiu, Q.-C. Zhuang, Q.-Q. Zhang, R. Cao, P.-Z. Ying, Y.-H. Qiang, and S.-G. Sun, "Electrochemical and electronic properties of LiCoO$_2$ cathode investigated by galvanostatic cycling and EIS," *Physical Chemistry Chemical Physics*, 2012.